Optics and Laser Technology 119 (2019) 105611

Contents lists available at ScienceDirect

Optics and Laser Technology

journal homepage: www.elsevier.com/locate/optlastec

Full length article

Ultrafast performance of all-optical AND and OR logic operations at 160 Gb/s using photonic crystal semiconductor optical amplifier

Amer Kotb[a,b,*], Kyriakos E. Zoiros[c], Chunlei Guo[a,d,*]

[a] The Guo China-US Photonics Laboratory, Changchun Institute of Optics, Fine Mechanics, and Physics, Chinese Academy of Sciences, Changchun 130033, China
[b] Department of Physics, Faculty of Science, University of Fayoum, Fayoum 63514, Egypt
[c] Lightwave Communications Research Group, Department of Electrical and Computer Engineering, School of Engineering, Democritus University of Thrace, Xanthi 67100, Greece
[d] The Institute of Optics, University of Rochester, Rochester, NY 14627, USA

HIGHLIGHTS

- All-optical AND and OR operations are analyzed at 160 Gb/s using PCSOA.
- Impact of critical operating parameters on QF is examined and assessed.
- All-optical operations using PCSOAs are more efficient than when using conventional SOAs.

ARTICLE INFO

Keywords:
All-optical AND operation
All-optical OR operation
Photonic crystal semiconductor optical amplifier
Mach-Zehnder interferometer
Delayed interferometer

ABSTRACT

The light confined and controlled by photonic crystals (PCs) can be exploited to enhance the performance and reduce the size of semiconductor optical amplifiers (SOAs) in which they are embedded. By incorporating PCSOAs in a Mach-Zehnder interferometer, or using a PCSOA followed by a delayed interferometer, Boolean AND and OR gates are formed, respectively, whose performance when executed all-optically (AO) is thoroughly analyzed at 160 Gb/s. For this purpose, the variation of the quality factor against the critical data signal and PCSOA operating factors is examined and assessed when the effects of amplified spontaneous emission and working temperature are included to make the simulation more realistic. The results obtained from the conducted theoretical study suggest that leveraging the PCSOAs benefits of low absorption loss, suppressed undesirable nonlinear effects, low power consumption, and high power transmission favors realizing the considered AO gates at the target data rate. Compared to conventional SOAs, PCSOAs advanced technology allows to obtain better logic performance, as quantified by the achieved higher metrics values, and to render the practical implementation of the AO gates more feasible, since the requirements for the PCSOAs structural parameters and driving conditions become more relaxed.

1. Introduction

Photonic crystals (PCs) are periodic dielectric structures that have a photonic band gap to confine and control the propagation of a range of light frequencies. This characteristic renders them appropriate for being exploited in the design of very small size optical modules. Additionally, PCs exhibit low absorption loss, suppressed undesirable nonlinear effects, low power consumption, and high power transmission over other nonlinear structures. These features make them attractive candidates for all-optical logic gates (AOLGs) purposes, which however is a possibility that has not widely been explored in the literature. On the other hand, conventional semiconductor optical amplifiers (SOAs) have extensively been used as nonlinear elements in AOLGs owing to their strong nonlinearity, compactness, power efficiency, and integration potential with other optoelectronic devices. However, employing SOAs at high operation speeds (> 100 Gb/s) is inherently difficult due to their finite gain recovery time [1–7]. Quantum dot (QD) SOAs, on the other hand, are capable of bypassing conventional SOAs slow gain dynamics [8–15], but their broad adoption and implementation in real applications still remain challenging due to practical issues. Thus, in

* Corresponding authors at: The Guo China-US Photonics Laboratory, Changchun Institute of Optics, Fine Mechanics, and Physics, Chinese Academy of Sciences, Changchun 130033, China.
E-mail addresses: amer@ciomp.ac.cn (A. Kotb), guo@optics.rochester.edu (C. Guo).

https://doi.org/10.1016/j.optlastec.2019.105611
Received 25 January 2019; Received in revised form 27 March 2019; Accepted 27 May 2019

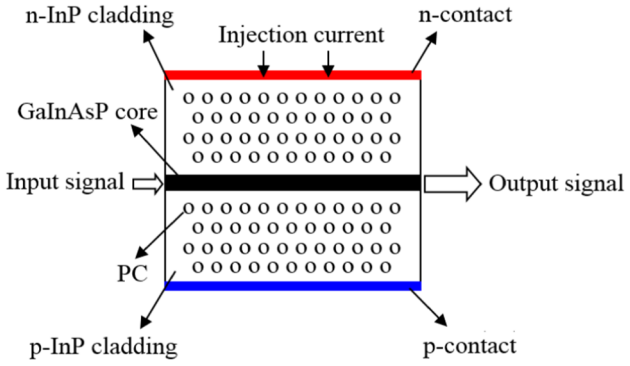

Fig. 1. Schematic diagram of PCSOA structure.

Table 1
Parameters default values used in numerical calculations.

Symbol	Definition	Value	Unit	Ref.
E_0	Pulse energy	30	fJ	[18]
τ_{FWHM}	Pulse width	1	ps	[17,18]
T	Bit period	6.25	ps	[29,17,18]
N	PRBS length	127	–	[30,31]
λ_A	Wavelength of data A (AND operation)	1580.4	nm	[32]
$\lambda_{delayed\ A}$	Wavelength of delayed A (AND operation)	1580.4	nm	[32]
λ_B	Wavelength of data B (AND operation)	1539.8	nm	[32]
P_A	Power of data A (AND operation)	0.4	mW	[32]
$P_{delayed\ A}$	Power of delayed A (AND operation)	0.4	mW	[32]
P_B	Power of data B (AND operation)	0.001	mW	[32]
$\Delta\tau$	Time delay (AND operation)	0.5	ps	–
λ_A	Wavelength of data A (OR operation)	1581	nm	[33,34]
λ_B	Wavelength of data B (OR operation)	1581	nm	[33,34]
λ_{CW}	Wavelength of CW (OR operation)	1540	nm	[33,34]
P_A	Power of data A (OR operation)	1	mW	[33,34]
P_B	Power of delayed A (OR operation)	1	mW	[33,34]
P_{CW}	Power of data B (OR operation)	2	mW	[33,34]
$\Delta\tau_{DI}$	DI delay (OR operation)	0.2	ps	–
$\Delta\Phi$	DI phase bias (OR operation)	π	rad	–
I	Injection current	10	mA	[35,36]
P_{sat}	Saturation power	25	mW	[18]
τ_c	Carrier lifetime	20	ps	[18]
α	Traditional linewidth enhancement factor	4	–	[35]
α_{CH}	Linewidth enhancement factor due to CH	1	–	[31]
α_{SHB}	Linewidth enhancement factor due to SHB	0	–	[21,22]
ε_{CH}	Nonlinear gain suppression factor due to CH	0.02	W^{-1}	[21,22]
ε_{SHB}	Nonlinear gain suppression factor due to SHB	0.02	W^{-1}	[30,31]
τ_{CH}	Temperature relaxation rate	0.3	ps	[30,31]
τ_{SHB}	Carrier-carrier scattering rate	0.1	ps	[30,31]
Γ	Confinement factor	0.15	–	[30,31]
a	Differential gain	2×10^{-16}	cm^{-3}	[17]
L	Length of PCSOA active layer	10	μm	[21]
d	Thickness of PCSOA active layer	0.3	μm	[17,18]
G_0	Unsaturated power gain	30	dB	–
R	Radiation loss	1500	cm^{-1}	[17,18]
n_g	Group index	100	–	[17,18]
B_0	Optical bandwidth	3	nm	[17,18]
υ	Optical frequency	1550	nm	[17,29]
N_{SP}	Spontaneous emission factor	2	–	[30,17,18]
T_{op}	Operating temperature	290	K	[37]

this paper, we propose to combine the advantages of PCs with those of SOAs to boost further the performance of AOLGs at high data rates. This is done at 160 Gb/s for PCSOA-based all-optical AND and OR gates,

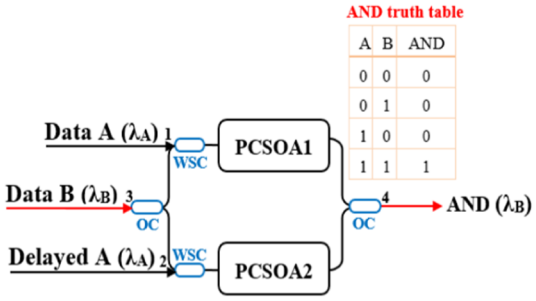

Fig. 2. Schematic diagram and truth table of AND gate using PCSOAs-MZI. OC: 3 dB optical coupler. WSC: wavelength selective coupler.

which are fundamental Boolean logic operations but so far have not been included in the suite of those operations that have theoretically been demonstrated using PCSOAs technology [16–18]. In this manner we continue, extend, and generalize our previous relevant research work on PCSOAs-based all-optical NOR and NAND gates [17,18]. The variation of the quality factor (QF) against the pulse energy and width, data rate, equivalent pseudorandom binary sequence (PRBS) length, group index, radiation loss, active region length and thickness, injection current, carrier lifetime, confinement factor, traditional linewidth enhancement factor, time delay for AND, and DI delay for OR, is examined and assessed, including the effect of amplified spontaneous emission (ASE) and operating temperature so as to obtain realistic results. For comparison, the impact of these parameters has been evaluated for both PCSOAs and conventional SOAs schemes at 160 Gb/s.

The rest of this paper is organized as follows: In Section 2, the PCSOA modeling is presented. In Section 3, the operation principle and simulation results of the AND gate are described. In Section 4, the operation principle and simulation results of the OR gate are given. Finally, the concluding remarks are given in Section 5.

2. PCSOA modeling

Fig. 1 shows the schematic diagram of the PCSOA structure. In this structure, the cladding layers are made of InP with a refractive index of 3.17, while the active (core) layer is made of GaInAsP with a refractive index of 3.45 [19]. The PCs are formed by the air holes passing vertically through the SOA structure. The PC has a radius of 0.158 μm, a depth of 2.3 μm, a lattice constant of 0.480 μm, and a vertical spacing between rows adjusted to 0.42 μm [18,20]. The PC waveguide works near the wavelength of 1.55 μm.

In this modeling, the input data signals A and B are assumed to be Gaussian-shaped whose power profiles are described by the following equation [21,22]:

$$P_{A,B}(t) \equiv P_{in}(t) = \sum_{n=1}^{N} a_{nA,B} \frac{2\sqrt{\ln[2]}\ E_0}{\sqrt{\pi}\ \tau_{FWHM}}\ exp\left[-\frac{4\ln[2](t-nT)^2}{\tau_{FWHM}^2}\right] \quad (1)$$

where $\alpha_{nA,B}$ is '0' or '1' inside a N bit-long pseudorandom binary sequence (PRBS) of pulses having energy E_0, full-width at half maximum (FWHM) pulse width τ_{FWHM}, and bit period T. The format of the input pulses used is return-to-zero (RZ), which is widely used in optical communications systems due to its attractive features of better tolerance to fiber nonlinearities and improved receiver sensitivity [23]. These pulses occupy only a fraction of the repetition interval to help avoid interference between adjacent allocated bit slots [24], and their generation while being as fast and short as in the study is technologically feasible with state-of-art lightwave sources [25].

The interband, which includes carrier depletion (CD), and intraband, which includes carrier heating (CH) and spectral hole burning (SHB), nonlinear effects are taken into account in this model. In particular, the CH process occurs on a time range between 0.1 and 0.7 ps due to carriers' thermalization in the entire energy band following the

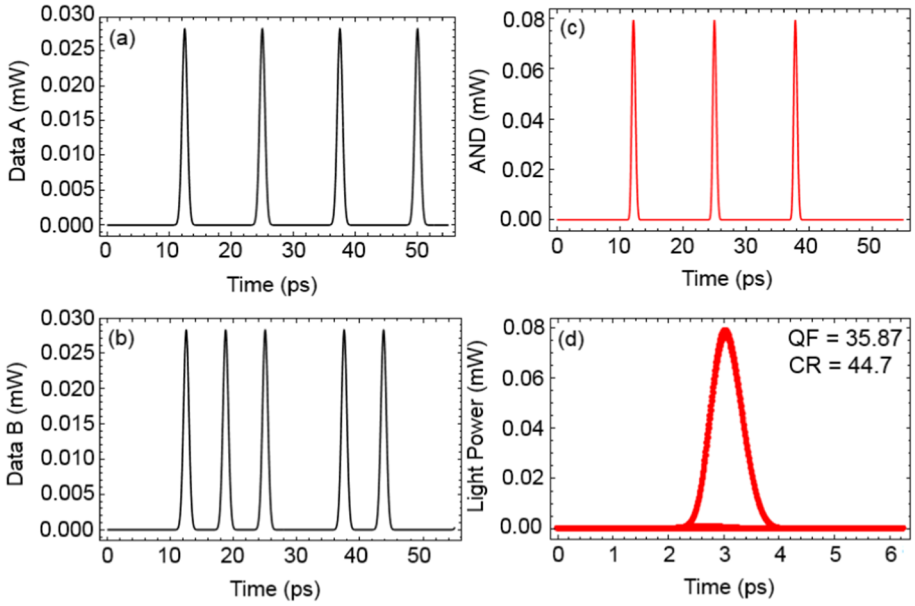

Fig. 3. AND simulation results using PCSOAs-MZI at 160 Gb/s. (a) Input data A, (b) input data B, (c) AND gate, and (d) corresponding eye diagram with QF of 35.87 and CR of 44.7.

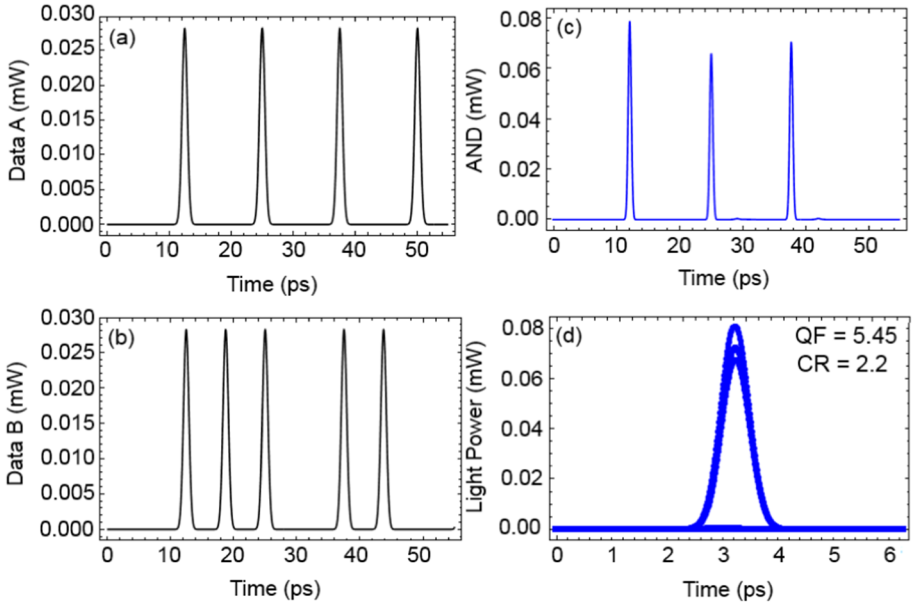

Fig. 4. AND simulation results using SOAs-MZI at 160 Gb/s. (a) Input data A, (b) input data B, (c) AND gate, and (d) corresponding eye diagram with QF of 5.45 and CR of 2.2.

pulse, while the SHB results when the pulse energy burns a hole in the gain spectrum. The time-dependent gain of each PCSOA is described by the following differential equations [17,18]:

$$\frac{dh_{CD}(t)}{dt} = \frac{h_0 - h_{CD}(t)}{\tau_C} - (Rv_g)h_{PC}[t] - (\exp[h_{CD}(t) + h_{CH}(t) + h_{SHB}(t)] - 1)\frac{P_{in}(t)}{E_{sat}} \quad (2)$$

$$\frac{dh_{PC}(t)}{dt} = \left(\frac{L\,R}{\tau_c}\right)(h_0 - h_{PC}(t)) - (Rv_g)h_{CD}(t) \quad (3)$$

$$\frac{dh_{CH}(t)}{dt} = -\frac{h_{CH}(t)}{\tau_{CH}} - \frac{\varepsilon_{CH}}{\tau_{CH}}(\exp[h_{CD}(t) + h_{CH}(t) + h_{SHB}(t)] - 1) P_{in}(t) \quad (4)$$

$$\frac{dh_{SHB}(t)}{dt} = -\frac{h_{SHB}(t)}{\tau_{SHB}} - \frac{\varepsilon_{SHB}}{\tau_{SHB}}(\exp[h_{CD}(t) + h_{CH}(t) + h_{SHB}(t)] - 1)P_{in}(t) - \frac{dh_{CD}(t)}{dt} - \frac{dh_{CH}(t)}{dt} \quad (5)$$

where functions h_{CD}, h_{PC}, h_{CH}, and h_{SHB} represent the gain of the PCSOA integrated over its length due to CD, PC, CH, and SHB, respectively. $h_0 = \ln[G_0]$, where G_0 is the unsaturated power gain. R is the radiation loss and v_g is the light group velocity, i.e., $v_g = c/n_g$, where c is the light speed in vacuum and n_g is the group index. Realistic values of these parameters are R = 30 cm^{-1} and n_g = 3 for a standard SOA, while R = 1500 cm^{-1} and n_g = 100 for a PCSOA [17,18,26]. E_{sat} is the saturation energy, which is related to the saturation power (P_{sat}) through $E_{sat} = P_{sat}\,\tau_c$, where τ_c is the carrier lifetime. τ_{CH} and τ_{SHB} are the temperature relaxation rate and carrier-carrier scattering rate, respectively. ε_{CH} and ε_{SHB} are the nonlinear gain suppression factors due to CH and SHB, respectively. The total optical gain of each PCSOA is

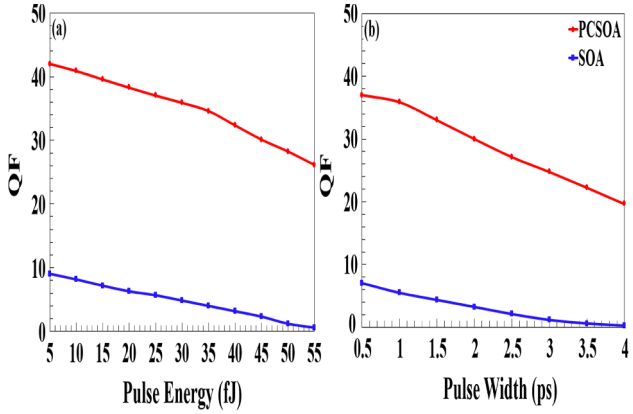

Fig. 5. QF vs. (a) pulse energy and (b) pulse width for AND operation using PCSOAs- and SOAs-based MZI at 160 Gb/s.

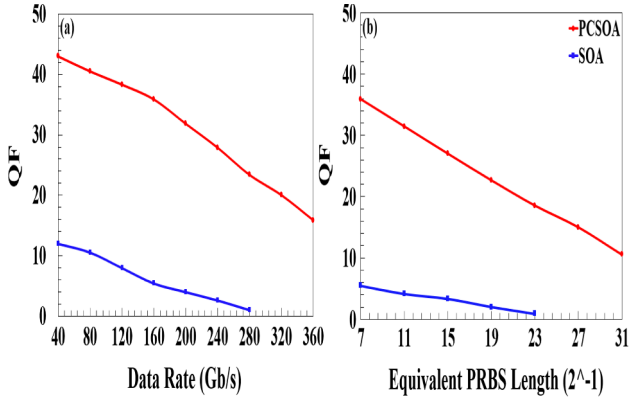

Fig. 6. QF vs. (a) data rate and (b) equivalent PRBS length for AND operation using PCSOAs- and SOAs-based MZI at 160 Gb/s.

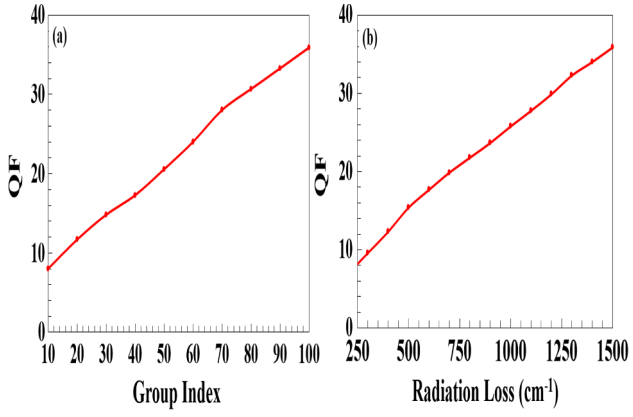

Fig. 7. QF vs. PCSOA (a) group index and (b) radiation loss for AND operation at 160 Gb/s.

formulated as [17,27]:

$$G_{PCSOA_{1,2}}(t) = exp\,[h_{CD}(t) + h_{CH}(t) + h_{SHB}(t)] \quad (6)$$

The induced phase change inside each PCSOA is given by [18,21]:

$$\Phi_{PCSOA_{1,2}}(t) = -0.5\,(\alpha\, h_{CD}(t) + \alpha_{CH} h_{CH}(t) + \alpha_{SHB} h_{SHB}(t)) \quad (7)$$

where α is the traditional linewidth enhancement factor (α-factor), α_{CH} is the linewidth enhancement factor due to CH, and α_{SHB} is the linewidth enhancement factor due to SHB. In this study, α_{SHB} is null because the SHB produces a nearly asymmetrical spectral hole centered at the signal wavelength [21,22]. The computational codes have been prepared and run in Mathematica®. The performance of the considered AOLGs has been evaluated through the QF, which is defined as $QF = (P_1 - P_0)/(\sigma_1 + \sigma_0)$ [17,18], where $P_{1,0}$ are the mean peak powers of the output logical '1's and '0's and $\sigma_{1,0}$ are the corresponding standard deviations. For acceptable performance, the QF must be over six so that the related bit error rate is smaller than 10^{-9} [21]. The QF is complemented by values of the contrast ratio (CR), which is defined as [28] $CR = P_1/P_0$. The higher this auxiliary metric the better the degree of switching achieved at the MZI output. The operating parameters of the input signal and PCSOA used in this study to realize the AND and OR operations have been cited in Table 1.

3. AND gate at 160 Gb/s

Fig. 2 shows the schematic diagram and truth table of the AND gate using PCSOAs-based MZI.

To realize AND operation, data signal A and its delayed version at the wavelength (λ_A) are injected into the PCSOAs-MZI upper and lower arms, respectively. Data signal B at a different wavelength (λ_B) is injected into PCSOAs-MZI middle arm and is split by a 3 dB optical coupler (OC) into two parts of equal (halved) intensity and relative phase difference 0.5π. Using wavelength selective couplers (WSCs), one part at λ_B is combined with direct data signal A at λ_A, while the other part, also at λ_B, is combined with delayed data signal A at λ_A to enter PCSOA1 and PCSOA2, respectively, as aggregate signals at $\lambda_A + \lambda_B$, which should lie within the PCSOAs gain bandwidth. Data signal A and its delayed copy incur a phase gate for data B [35]. When A = '0', this phase gate does not exist for B = '1' or '0' and the output is '0'. When both A = B = '1', the phase gate allows the first OC-split components of data B = '1' to interfere constructively, i.e. by integer multiples of 2π, at a second OC identical to the first, which recombines the signal constituents coming from its two input ports with 50% power coupling ratio and phase shift of 0.5π for signals that pass through its passive configuration in cross input-output direction [38]. Thus the binary outcome produced in this case is '1'. This means that the PCSOAs-MZI output is '1' only when A = B = '1', which is functionally the AND operation whose result is obtained at λ_B after filtering (not shown in Fig. 2). It must be noted that the AO AND logic scheme used in this paper differs from [18] in that PCSOA2 is excited by the delayed version of data signal A, whilst in [18] the corresponding active element is driven by a continuous wave auxiliary signal to balance the gain and subsequently phase mismatch between the two MZI arms when the binary content of A is null. This essentially means that the AND gate implementation applied in the present paper exhibits less complexity, power consumption and cost, overall better practicality, and feasibility than that in [18].

The input pulses powers inserted in the PCSOAs-MZI for the AND operation are described as [27,39]:

$$P_{in,PCSOA_1}(t) = P_A(t) + 0.5P_B(t) \quad (8)$$

$$P_{in,PCSOA_2}(t) = 0.5P_B(t) + P_A(t - \Delta\tau) \quad (9)$$

where the coefficient '0.5' refers to the halving of data B via 3 dB OC. Δτ is the time delay of a delayed signal A.

The time-dependent AND output power at port 4 of the PCSOAs-MZI is given by [18,21,22,40]:

$$P_{AND,MZI}(t) = 0.25P_B(t)\,(G_{PCSOA_1}(t) + G_{PCSOA_2}(t) - 2\sqrt{G_{PCSOA_1}(t)\,G_{PCSOA_2}(t)}\,\cos\,[\Phi_{PCSOA_1}(t) - \Phi_{PCSOA_2}(t)]) \quad (10)$$

Figs. 3 and 4 show the pulses profile and corresponding eye diagrams for the AND operation at 160 Gb/s using PCSOAs- and conventional SOAs-based MZI, respectively. The achieved QF values are 35.87 and 5.45 using PCSOAs- and SOAs-based MZI, respectively. The corresponding CR values are 44.7 and 2.2. These figures show that the AND

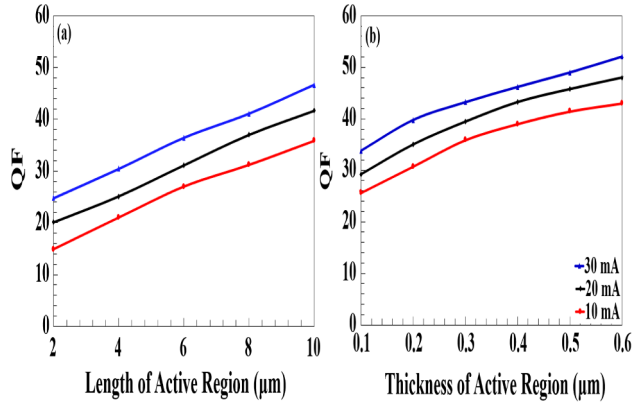

Fig. 8. QF vs. PCSOA active region (a) length and (b) thickness for AND operation at 160 Gb/s for I = 10, 20, and 30 mA.

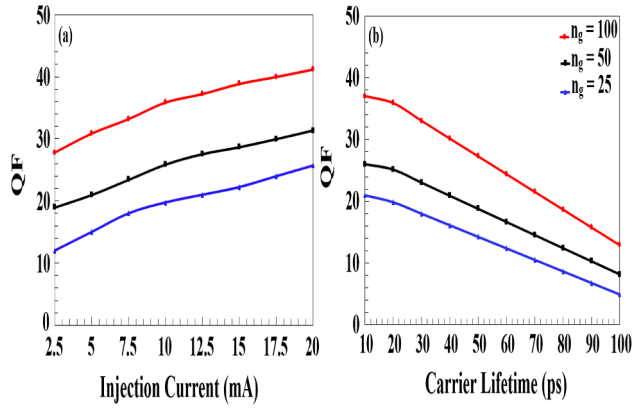

Fig. 9. QF vs. PCSOA (a) injection current and (b) carrier lifetime for AND operation at 160 Gb/s for n_g = 25, 50, and 100.

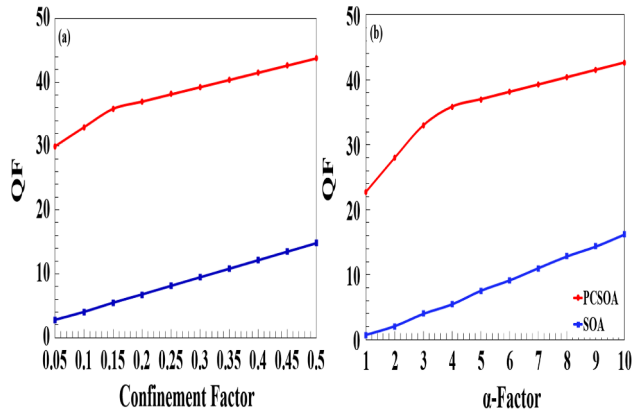

Fig. 10. QF vs. (a) confinement factor and (b) traditional linewidth enhancement factor (α-factor) for AND gate using PCSOAs- and SOAs-based MZI at 160 Gb/s.

operation can be executed at 160 Gb/s using PCSOAs with no pulse amplitude fluctuations due to pattern effects, with clear and distortionless eye diagram and with a much higher QF than when using conventional SOAs for the same purpose.

Figs. 5 and 6 show the QF versus the pulse energy, pulse width, data rate, and equivalent PRBS length. For comparison, these results have been obtained for PCSOAs- and conventional SOAs-based schemes at 160 Gb/s. Fig. 5 confirms that more energetic pulses cause a (PC)SOA saturation that degrades the output QF. Still, the QF obtained using PCSOAs is more tolerant to the variations of this parameter than when using conventional SOAs. On the other hand, the QF drops with the increase of the operating data rate, as shown in Fig. 6(a), but its value is still acceptable when using PCSOAs even up to 360 Gb/s, while this is possible for less than a half data rate, i.e. ~160 Gb/s, when using SOAs. A similar qualitative trend is observed in Fig. 6(b) for the QF versus the equivalent PRBS length [30,31], which implies that the PCSOA-based AOLGs can support operation for longer PRBS than conventional SOA-based.

Fig. 7 shows the dependence of the QF on the PCSOAs group index and radiation loss for the AND at 160 Gb/s. A large group index enhances the light-matter interaction and therefore increases the output QF, as shown in Fig. 7(a). The radiation loss increases with the thickness of PCSOA layers and with decreasing the depth of PC holes. Thus, the PC holes depth should be formed with sufficient depth, which is 2.3 μm in our case. Fig. 7(b) shows that the QF increases with radiation loss. This result indicates that these losses are sufficiently compensated in PCSOAs due to their larger gain achieved at much lower injection currents than conventional SOAs [18,26].

Fig. 8 shows the QF as a function of the length and thickness of the PCSOA active region for the AND operation at 160 Gb/s. This figure has been obtained after making numerical adjustments with the PCSOA injection currents, i.e., I = 10, 20, and 30 mA. The materials and structure used in the conventional SOA are the same as used in the PCSOA. This figure shows that the QF increases for longer and thicker PCSOA active region because of the enhanced light-matter interactions in the PCSOA structure. The PCSOA total size is smaller than a conventional SOA. This result indicates that the PCSOA-based AOLGs can be more compact in size than with conventional SOA and hence be more easily adjustable for integration.

Fig. 9 shows the dependence of the QF on the PCSOA injection current (I) and carrier lifetime (τ_c) for the AND operation at 160 Gb/s for different group indices (n_g), i.e., 25, 50, and 100. For acceptable performance, the PCSOA needs much lower injection current than the conventional SOA. For I = 10 mA, the output QF using PCSOA is 35.87. Therefore, the PCSOA is more suitable as a nonlinear device for AOLGs with both acceptable performance and higher QF than the conventional SOA. Since τ_c determines the speed of gain recovery, the QF becomes higher for smaller values of this parameter as shown in Fig. 9(b).

The variation of the QF against the confinement factor (Γ) and traditional linewidth enhancement factor (α-factor) for the AND gate at 160 Gb/s using PCSOAs- and SOAs-based MZI is shown in Fig. 10. For low Γ, less energy of the waveguide mode is confined into the active layer, which affects the (PC)SOA saturation level required for proper switching and decreases the QF. The output QF is increased with Γ for both devices, as shown in Fig. 10(a). The nonlinear light-matter interactions are stronger for the PCSOA than the conventional SOA [19]. Similar behavior is observed for the QF versus α-factor in Fig. 10(b), where the performance of the AND gate with PCSOA is acceptable even for small values of α-factor compared to SOA. α-factor is related according to Eq. (7) to the integrated gain response, which hence is stronger in the PCSOA than in SOA, so the phase shift is more efficient in the former than in the latter case.

Fig. 11 shows the QF versus the time offset of delayed signal A (Δτ) for the AND operation at 160 Gb/s using PCSOAs- and SOAs-based MZI. The time delay between signal A and its delayed replica creates a switching phase gate for signal B, so the phase change of the latter depends on this parameter. The highest QF is achieved at the optimum of Δτ = 0.5 ps. This figure confirms that the QF using PCSOA remains acceptable across the whole scanned span, which in turn becomes narrower for the conventional SOA.

For realistic results, the effect of the amplified spontaneous emission (ASE) and operating temperature on the QF have been taken into account. The ASE causes a degradation of the gates performance, so it acts as noise on the optical amplifiers. The ASE power is related to the spontaneous emission factor (N_{sp}) through $P_{ASE} = N_{SP}(2\pi\hbar(G_0 - 1))\upsilon B_0$ [37,41,42], where ħ is normalized Planck's

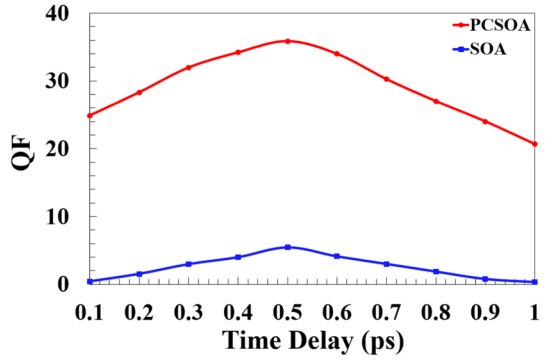

Fig. 11. QF vs. time delay of delayed A for AND gate using PCSOAs- and SOAs-based MZI at 160 Gb/s.

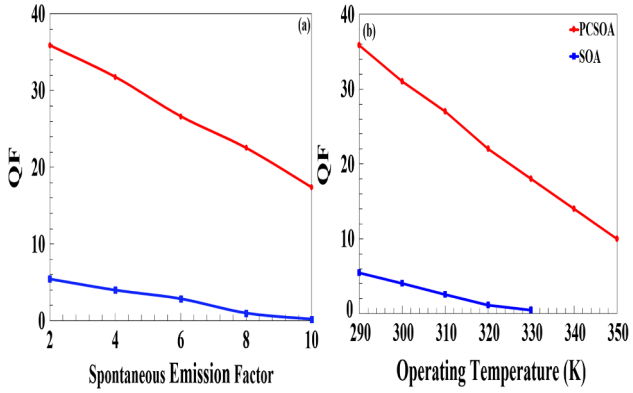

Fig. 12. QF vs. (a) spontaneous emission factor and (b) operating temperature for AND gate using PCSOAs- and SOAs-based MZI at 160 Gb/s.

constant, υ is the optical frequency, and B_0 is the optical bandwidth. The ASE is numerically added to the gates' output power using the above expression. The QF versus N_{sp} for the AND operation at 160 Gb/s using PCSOA- and SOA-based MZI is shown in Fig. 12(a). It can be clearly seen that the performance of the AND gate using PCSOA is not highly affected by ASE noise and remains acceptable even at higher N_{sp} values. On the other hand, a reduction in operating temperature speeds-up the gain recovery time of the (PC)SOA [2], which results in an increase of the QF, as shown in Fig. 12(b). Physically, the probability of occupation of active region energy levels increases with a decrease in device operating temperature. Furthermore, the number of carriers available for providing optical gain are distributed over a narrow range at a lower temperature. Also, the nonradiative recombinations decrease with a decrease in temperature and hence cause an increase in gain [21]. The device operating temperature can be controlled through its power supply unit or on-chip thermoelectric cooling unit. Overall, the performance of the AND Boolean function using PCSOA is more acceptable than SOA even at higher temperatures.

4. OR gate at 160 Gb/s

Fig. 13 shows the schematic diagram and truth table for the OR gate using PCSOA-based DI.

For OR operation, data streams A, B, and a continuous wave (CW) 'probe' signal are combined and injected into a single PCSOA. Data A and B play the main role in inducing on the CW beam a phase shift via the (PC)SOA cross-phase modulation nonlinear effect [43]. The CW signal coming out from PCSOA is split into two parts of equal intensity via an OC, which are injected into the two arms of a DI. The DI creates a phase difference between the CW constituents by adjustment of its critical operation parameters, i.e., the delay ($\Delta\tau_{DI}$) and the phase bias ($\Delta\Phi$). Thus, when both A and B are '0′, no phase change is imparted on the CW signal, which results in '0′ at the DI output. On the other hand, when A or B, or both, are '1′, the CW acquires phase changes and its direct and lagging counterparts interfere destructively, which results in '1′ at the DI output. In this manner, the OR operation is realized.

For OR operation, the input power inserted in the PCSOA is defined as [44]:

$$P_{in,PCSOA}(t) = P_A(t) + P_B(t) + P_{CW} \tag{11}$$

The time-dependent output power of the PCSOA-DI is given by [44]:

$$P_{OR,DI}(t) = 0.25\begin{pmatrix} P_{out,PCSOA}(t) + P_{out,PCSOA}(t-\Delta\tau_{DI}) - \\ 2\sqrt{P_{out,PCSOA}(t)\,P_{out,PCSOA}(t-\Delta\tau_{DI})} \\ \cos\left[\Phi_{out,PCSOA}(t) - \Phi_{out,PCSOA}(t-\Delta\tau_{DI}) + \Delta\Phi\right] \end{pmatrix} \tag{12}$$

The pulses profile and corresponding eye diagrams for the OR operation at 160 Gb/s using PCSOA- and SOA-based DI are shown in Figs. 14 and 15, respectively. The values of the parameters used in these calculations are cited in Table 1. It is clearly seen that the QF with PCSOA is higher and more than acceptable than with SOA, i.e. 23 vs. 5.2. The CR values are also higher with PCSOA than with SOA, i.e. 13.46 vs. 2.1. Physically this happens because the single SOA used to carry out the OR gate undergoes a deep saturation due to the simultaneous insertion of three different signals, which makes it hard for the gain to timely recover and for data pulses to encounter the same response. On the other hand, with PCSOA the gain recovery due to high light-matter interactions is enhanced to the point that the respective pulses emerge with uniform logic amplitudes.

The variation of the QF against the signal key parameters, i.e. energy, width, data rate, and equivalent PRBS length, for the OR gate at 160 Gb/s using PCSOA- and SOA-based DI is shown, respectively, in Figs. 16 and 17. Still, the performance of the OR function based on PCSOA-DI is more acceptable than when using a conventional SOA-DI. Furthermore, for high values of those parameters, the OR output QF using SOA becomes a negative value.

The dependence of the OR QF on the PCSOA physical and structural parameters has been examined in this part. Fig. 18 shows the QF as a function of the PCSOA group index and radiation loss for the OR operation at 160 Gb/s.

The variation of the OR QF against the length and thickness of the PCSOA active region for I = 10, 20, and 30 mA at 160 Gb/s is shown in

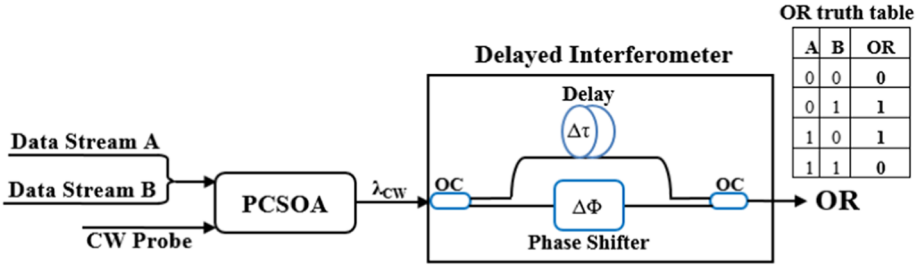

Fig. 13. Schematic diagram and truth table for OR gate using PCSOA-based DI. OC: 3 dB optical coupler.

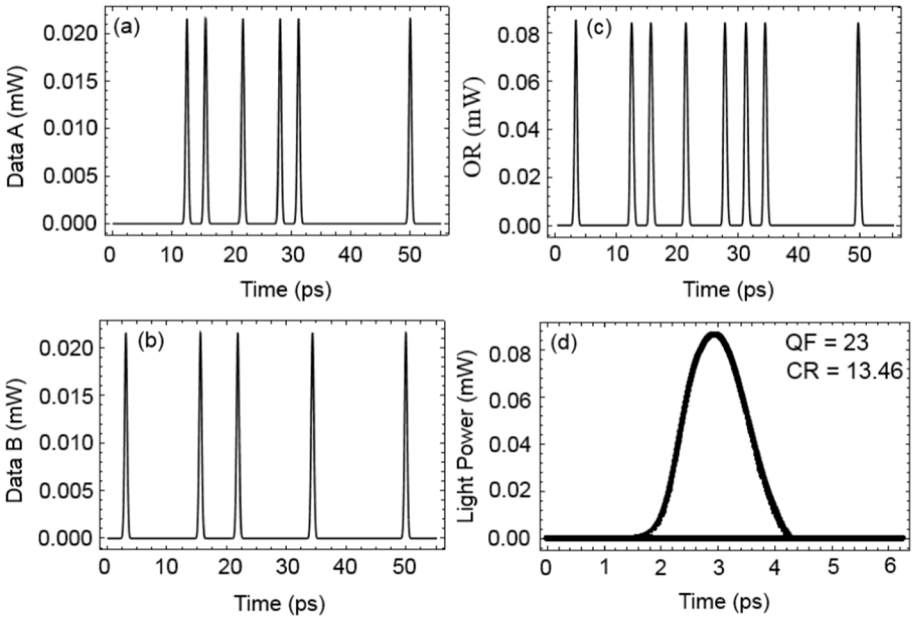

Fig. 14. OR simulation results using PCSOA-DI at 160 Gb/s. (a) Input data A, (b) input data B, (c) OR gate, and (d) corresponding eye diagram with QF of 23 and CR of 13.46.

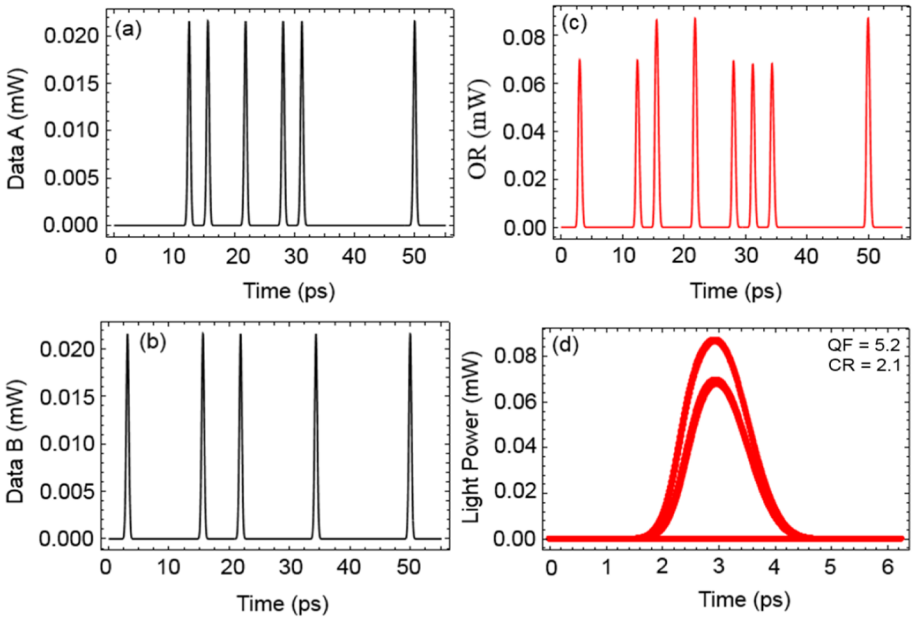

Fig. 15. OR simulation results using SOA-DI at 160 Gb/s. (a) Input data A, (b) input data B, (c) OR gate, and (d) corresponding eye diagram with QF of 5.2 and CR of 2.1.

Fig. 19.

Fig. 20 shows the QF versus the PCSOA injection current and carrier lifetime for the OR operation at 160 Gb/s for n_g = 25, 50, and 100.

Fig. 21 shows the QF dependence on the confinement factor (Γ) and traditional linewidth enhancement factor (α-factor) for the OR function at 160 Gb/s using PCSOA- and SOA-based DI.

The value of the QF for the OR operation is very sensitive to the DI delay ($\Delta\tau_{DI}$). As shown in Fig. 22, for low DI delays, the QF decreases because a destructive interference occurs at the DI output. For high DI delays, the QF decreases again because the side pulses start moving into the neighboring bit slots [45]. An optimum QF of 23 using a PCSOA has been achieved at a DI delay of 0.2 ps. The performance of OR operation using a PCSOA is more than acceptable across the whole scanned span than when using a SOA.

The QF of the OR operation within a PCSOA- and SOA-based DI at 160 Gb/s decreases with increasing N_{sp} and operating temperature as shown, respectively, in Fig. 23(a) and (b).

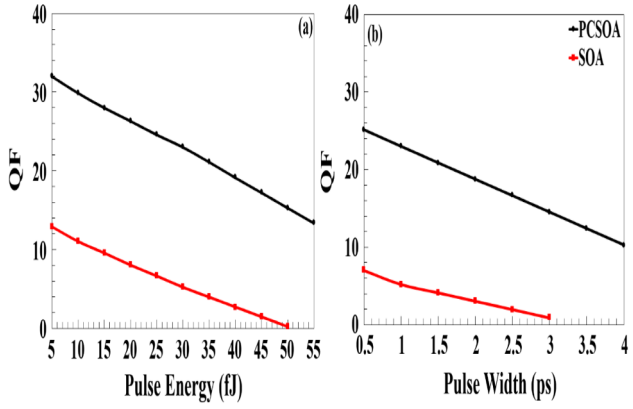

Fig. 16. QF vs. (a) pulse energy and (b) pulse width for OR operation using PCSOA- and SOA-based DI at 160 Gb/s.

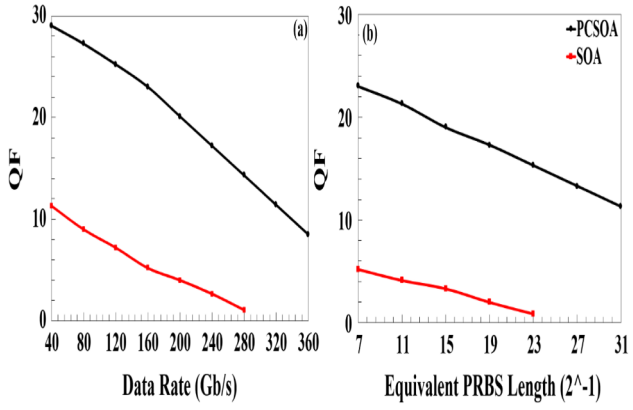

Fig. 17. QF vs. (a) data rate and (b) equivalent PRBS length for OR operation using PCSOA- and SOA-based DI at 160 Gb/s.

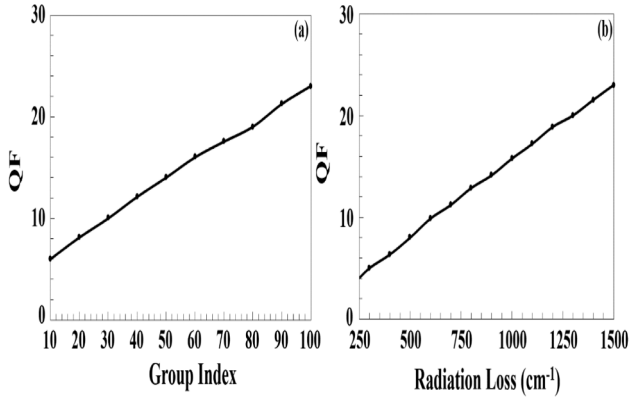

Fig. 18. QF vs. PCSOA (a) group index and (b) radiation loss for OR operation at 160 Gb/s.

5. Conclusion

The ultrafast performance of all-optical AND and OR functions with photonic crystal semiconductor optical amplifiers (PCSOAs), which are incorporated in a Mach-Zehnder interferometer for AND, or combined with a delayed interferometer, for OR, was theoretically investigated and analyzed at 160 Gb/s. For comparison, the results were obtained

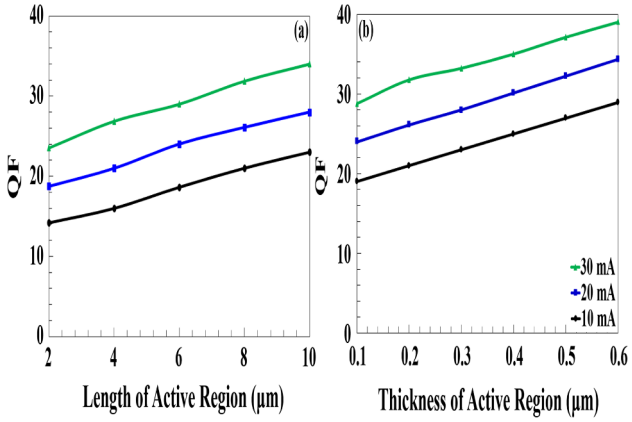

Fig. 19. QF vs. PCSOA active region (a) length and (b) thickness for OR operation at 160 Gb/s for I = 10, 20, and 30 mA.

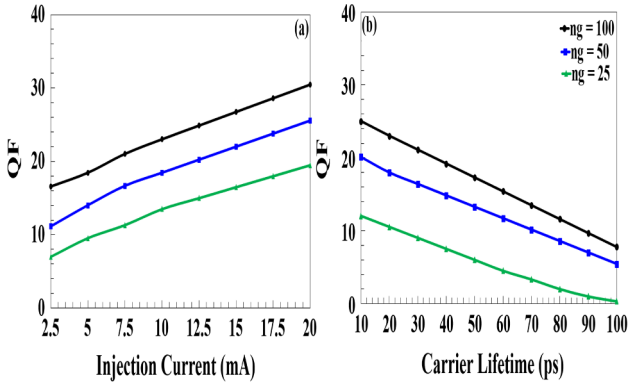

Fig. 20. QF vs. PCSOA (a) injection current and (b) carrier lifetime for OR operation at 160 Gb/s for n_g = 25, 50, and 100.

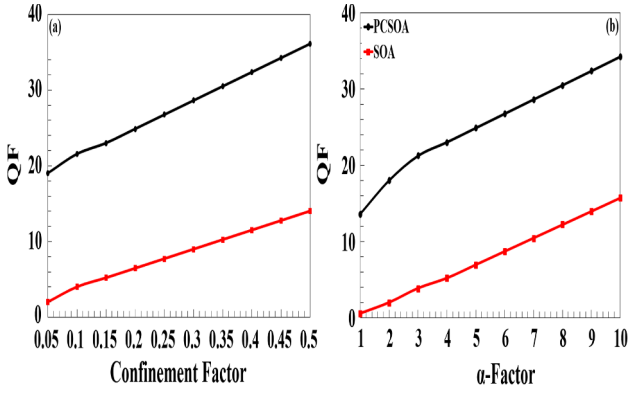

Fig. 21. QF vs. (a) confinement factor and (b) traditional linewidth enhancement factor (α-factor) for OR using PCSOA- and SOA-based DI at 160 Gb/s.

for the PCSOAs and conventional SOAs schemes at 160 Gb/s. The variation of the gates' quality factor against the input pulse and (PC)SOA key parameters was examined, including the impact of amplified spontaneous emission and operating temperature so as to obtain realistic results. The results indicate that these gates can be implemented with better performance, as quantified by the achieved higher metrics values, and in a more feasible manner, since the requirements for the

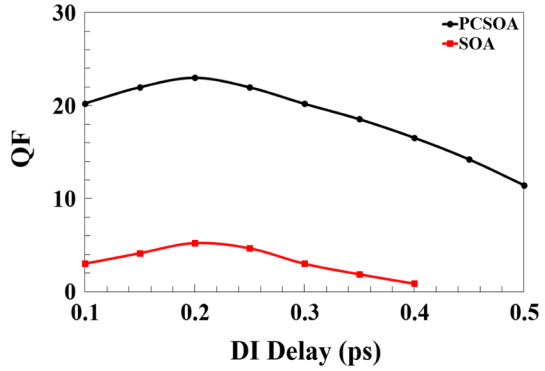

Fig. 22. QF vs. DI delay for OR gate using PCSOA- and SOA-based DI at 160 Gb/s.

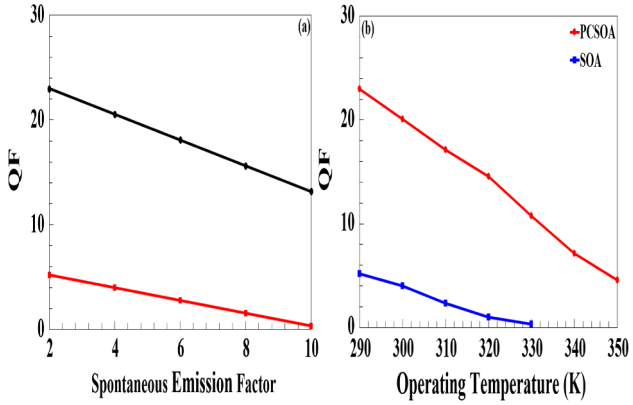

Fig. 23. QF vs. (a) spontaneous emission factor and (b) operating temperature for OR gate using PCSOA- and SOA-based DI at 160 Gb/s.

PCSOAs structural parameters and driving conditions become more relaxed, compared to conventional SOA technology.

Acknowledgment

This work was funded by the Chinese Academy of Sciences President's International Fellowship Initiative (Grant No. 2019FYT0002) and Talented Young Scientist Program supported by the China Science and Technology Exchange Center of Ministry of Science and Technology of China.

References

[1] C. Qin, J. Zhao, H. Yu, J. Zhang, Gain recovery dynamics in semiconductor optical amplifiers with distributed feedback grating under assist light injection, Opt. Eng. 55 (2016) 076116.
[2] Y. Kumar, M.R. Shenoy, Enhancement in the gain recovery of a semiconductor optical amplifier by device temperature control, Pramana J. Phys. 87 (2016) 1–6.
[3] Y. Kumar, M.R. Shenoy, A novel scheme of optical injection for fast gain recovery in semiconductor optical amplifier, IEEE Photon. Technol. Lett. 26 (2014) 933–936.
[4] C. Li, X. Tian, Z. Xiu, Z. Shang, G. Xiao, T. Xiao, L. Yong, Theoretical analysis of ultra-fast phase recovery in semiconductor optical amplifiers, Chin. Sci. Bulletin 57 (2012) 1078–1082.
[5] F. Ginovart, J.C. Simon, I. Valiente, Gain recovery dynamics in semiconductor optical amplifier, Opt. Commun. 199 (2011) 111–115.
[6] R. Giller, R.J. Manning, G. Talli, R.P. Webb, M.J. Adams, Analysis of the dimensional dependence of semiconductor optical amplifier recovery speeds, Opt. Exp. 15 (2007) 1773–1782.
[7] R. Giller, R.J. Manning, D. Cotter, Gain and phase recovery of optically excited semiconductor optical amplifiers, IEEE Photon. Technol. Lett. 18 (2006) 1061–1063.
[8] Y. Ben-Ezra, B.I. Lembrikov, M. Haridim, Ultrafast all-optical processor based on quantum-dot semiconductor optical amplifiers, IEEE J. Quant. Electron. 45 (2009) 34–41.
[9] M. Sugawara, T. Akiyama, N. Hatori, Y. Nakata, H. Ebe, H. Ishikawa, Quantum-dot semiconductor optical amplifiers for high-bit-rate signal processing up to 160Gbs−1 and a new scheme of 3R regenerators, Meas. Sci. Technol. 13 (2002) 1683–1689.
[10] Y. Ben-Ezra, M. Haridim, B.I. Lembrikov, Theoretical analysis of gain-recovery time and chirp in QD-SOA, IEEE Photon. Technol. Lett. 17 (2005) 1803–1805.
[11] S. Ma, Z. Chen, H. Sun, N.K. Dutta, High-speed all-optical logic gates based on quantum-dot semiconductor optical amplifiers, Opt. Exp. 18 (2010) 6417–6422.
[12] A. Kotb, K.E. Zoiros, On the design of all-optical gates based on quantum-dot semiconductor optical amplifier with effect of amplified spontaneous emission, Opt. Quant. Electron. 46 (2014) 977–989.
[13] A. Rostami, H. Nejad, R. Qartavol, H. Saghai, Tb/s optical logic gates based on quantum-dot semiconductor optical amplifiers, IEEE J. Quant. Electron. 46 (2010) 354–360.
[14] A. Kotb, Simulation of high-quality-factor all-optical logic gates based on quantum-dot semiconductor optical amplifier at 1 Tb/s, Optik 126 (2016) 320–325.
[15] A. Kotb, K.E. Zoiros, C. Guo, 2 Tb/s all-optical gates based on two-photon absorption in quantum dot semiconductor optical amplifiers, Opt. Laser Technol. 112 (2019) 442–451.
[16] H. Taleb, K. Abedi, Design of a novel low power all-optical NOR gate using photonic crystal quantum-dot semiconductor optical amplifiers, Opt. Lett. 39 (2014) 6237–6241.
[17] A. Kotb, K.E. Zoiros, Performance analysis of all-optical XOR gate with photonic crystal semiconductor optical amplifier-assisted Mach-Zehnder interferometer at 160 Gb/s, Opt. Commun. 402 (2017) 511–517.
[18] A. Kotb, K.E. Zoiros, C. Guo, 160 Gb/s photonic crystal semiconductor optical amplifiers-based all-optical logic NAND gate, Photon. Netw. Commun. 36 (2018) 246–255.
[19] A. Nosratpour, M. Razaghi, G. Darvish, Computational study of pulse propagation in photonic crystal semiconductor optical amplifier, J. Nanophoton. 12 (2018) 036015.
[20] T. Cao, Y.L.D. Ho, P.J. Heard, L.P. Barry, A.E. Kelly, M.J. Cryan, Fabrication and measurement of a photonic crystal waveguide integrated with a semiconductor optical amplifier, J. Opt. Soc. Am. B 26 (2009) 768–777.
[21] N.K. Dutta, Q. Wang, Semiconductor optical amplifiers, second ed., World Scientific Publishing Company, Singapore, 2013.
[22] A. Kotb, All-optical logic gates using semiconductor optical amplifier, Lambert Academic Publishing, Saarbrucken, 2012.
[23] D. Breuer, K. Petermann, Comparison of NRZ- and RZ-modulation format for 40-Gb/s TDM standard-fiber systems, IEEE Photon. Technol. Lett. 9 (1997) 398–400.
[24] S. Kawanishi, Ultrahigh-speed optical time-division-multiplexed transmission technology based on optical signal processing, IEEE J. Quant. Electron. 34 (1998) 2064–2079.
[25] G. Zhu, Q. Wang, H. Chen, H. Dong, N.K. Dutta, High-quality optical pulse train generation at 80 Gb/s using a modified regenerative-type mode-locked fiber laser, IEEE J. Quant. Electron. 40 (2004) 721–725.
[26] E. Mizuta, H. Watanabe, T. Baba, All semiconductor low-Δ photonic crystal waveguide for semiconductor optical amplifier, Jap. J. Appl. Phys. 45 (2006) 6116–6120.
[27] A. Kotb, K.E. Zoiros, Soliton all-optical logic AND gate with semiconductor optical amplifier-assisted Mach-Zehnder interferometer, Opt. Eng. 55 (2016) 1–7.
[28] K.E. Zoiros, G. Papadopoulos, T. Houbavlis, G.T. Kanellos, Theoretical analysis and performance investigation of ultrafast all-optical Boolean XOR gate with semiconductor optical amplifier-assisted Sagnac interferometer, Opt. Commun. 258 (2006) 114–134.
[29] I. Rendón-Salgado, R. Gutiérrez-Castrejón, 160 Gb/s all-optical AND gate using bulk SOA turbo–switched Mach-Zehnder interferometer, Opt. Commun. 399 (2017) 77–86.
[30] A. Kotb, K.E. Zoiros, C. Guo, All-optical XOR, NOR, and NAND logic functions with parallel semiconductor optical amplifier-based Mach-Zehnder interferometer modules, Opt. Laser Technol. 108 (2018) 426–433.
[31] A. Kotb, K.E. Zoiros, C. Guo, Performance investigation of 120 Gb/s all-optical logic XOR gate using dual reflective semiconductor optical amplifier-based scheme, J. Comp. Electron. 17 (2018) 1640–1649.
[32] I. Rendón-Salgado, E. Ramírez-Cruz, R. Gutiérrez-Castrejón, 640 Gb/s all-optical AND gate and wavelength converter using bulk SOA turbo–switched Mach-Zehnder interferometer with improved differential scheme, Opt. Laser Technol. 109 (2019) 671–681.
[33] J.Y. Kim, J.M. Kang, T.Y. Kim, S.K. Han, All-optical multiple logic gates with XOR, NOR, OR and NAND function using parallel SOA-MZI structures: theory and experiment, J. Lightwave Technol. 24 (2006) 3392–3399.
[34] J. Dong, X. Zhang, J. Xu, D. Huang, 40 Gb/s all-optical logic NOR and OR gates using a semiconductor optical amplifier: experimental demonstration and theoretical analysis, Opt. Commun. 281 (2008) 1710–1715.
[35] H. Dong, Q. Wang, G. Zhu, J. Jaques, A.B. Piccirilli, N.K. Dutta, Demonstration of all-optical logic OR gate using semiconductor optical amplifier-delayed interferometer, Opt. Commun. 242 (2004) 479–485.
[36] Q. Wang, H. Dong, G. Zhu, H. Sun, J. Jaques, A.B. Piccirilli, N.K. Dutta, All-optical logic OR gate using SOA and delayed interferometer, Opt. Commun. 260 (2006) 81–86.
[37] A. Kotb, K.E. Zoiros, C. Guo, Numerical investigation of all-optical logic OR gate at 80 Gb/s with dual pump-probe semiconductor optical amplifier (SOA)-assisted Mach-Zehnder interferometer (MZI), J. Comp. Electron. 18 (2019) 271–278, https://doi.org/10.1007/s10825-018-1275-9.
[38] A. Yariv, Universal relations for coupling of optical power between microresonators and dielectric waveguides, Electron. Lett. 36 (2000) 321–322.
[39] H. Dong, H. Sun, Q. Wang, N.K. Dutta, J. Jaques, 80 Gb/s all-optical logic AND operation using Mach-Zehnder interferometer with differential scheme, Opt.

Commun. 265 (2006) 79–83.
[40] H. Dong, H. Sun, Q. Wang, N.K. Dutta, J. Jaques, All-optical logic AND operation at 80 Gb/s using semiconductor optical amplifier based Mach-Zehnder interferometer, Microwave Opt. Technol. Lett. 48 (2006) 1672–1675.
[41] A. Kotb, S. Ma, Z. Chen, N.K. Dutta, G. Said, Effect of amplified spontaneous emission on semiconductor optical amplifier based all-optical logic, Opt. Commun. 284 (2011) 5798–5803.
[42] A.M. Melo, K. Petermann, On the amplified spontaneous emission noise modeling of semiconductor optical amplifiers, Opt. Commun. 281 (2008) 4598–4605.
[43] S. Singh, R. Kaur, R.S. Kaler, Photonic processing for all-optical logic gates based on semiconductor optical amplifier, Opt. Eng. 53 (2014) 116102.
[44] A. Kotb, Ultrafast all-optical logic OR gate based on two-photon absorption with a semiconductor optical amplifier-assisted delayed interferometer, Korean Phys. Soc. 68 (2016) 201–205.
[45] S. Randel, A.M. Melo, K. Petermann, V. Marembert, C. Schubert, Novel scheme for ultrafast all-optical XOR operation, J. Lightwave Technol. 22 (2004) 2808–2815.